analytical chemistry

Article

pubs.acs.org/ac

Surface Plasmon Resonance Sensor Based on Magnetic Molecularly Imprinted Polymers Amplification for Pesticide Recognition

Gui-Hong Yao, Ru-Ping Liang, Chun-Fang Huang, Ying Wang, and Jian-Ding Qiu*

Department of Chemistry, Nanchang University, Nanchang, Jiangxi 330031, P. R. China

Supporting Information

ABSTRACT: We reported here a method to enhance detection sensitivity in surface plasmon resonance (SPR) spectroscopy integrated with a surface molecular imprinting recognition system and employing magnetic molecular imprinting polymer nanoparticles for amplifying SPR response. The proposed magnetic molecular imprinting polymer was designed by self-polymerization of dopamine on the Fe_3O_4 NPs surface in weak base aqueous solution in the presence of template chlorpyrifos (CPF). The imprinted Fe_3O_4@polydopamine nanoparticles (Fe_3O_4@PDA NPs) were characterized by Fourier transform infrared spectroscopy, UV−vis absorption spectroscopy, and transmission electron microscopy. The biosensor showed a good linear relationship between the SPR angle shift and the chlorpyrifos concentration over a range from 0.001 to 10 μM with a detection limit of 0.76 nM. A significant increase in sensitivity was therefore afforded through the use of imprinted Fe_3O_4@PDA NPs as an amplifier, and meanwhile, the imprinted Fe_3O_4@PDA NPs had an excellent recognition capacity to chlorpyrifos over other pesticides. The excellent sensitivity and selectivity and high stability of the designed biosensor make this magnetic imprinted Fe_3O_4@PDA NP an attractive recognition element for various SPR sensors for detecting pesticide residuals and other environmentally deleterious chemicals.

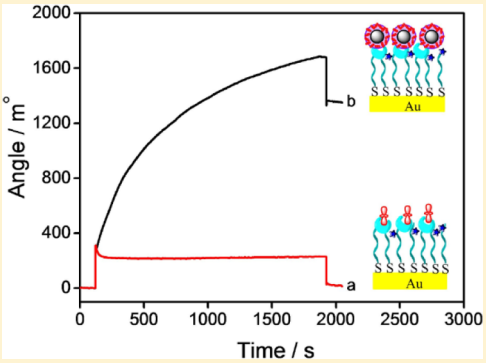

Organophosphate pesticides (OPs) have played an important role in increasing agricultural productivity. However, their excessive use in pre- and postharvest treatments to control diseases of fruits and vegetables may cause widespread contamination of air, water, soil, and agricultural products, eventually leading to long-term accumulation in ecosystems including humans.[1,2] The high toxicity of OPs results from irreversible binding to acetylcholinesterase (AChE) and thus inflicts serious harm to the human nervous system, respiratory tract, and cardiovascular system.[2] Up to now, many techniques including gas chromatography with mass spectrometry[3] and liquid chromatography with mass spectrometry techniques[4,5] have been utilized to monitor trace levels of these compounds. Although these methods are accurate in the identification of OPs, there are some drawbacks such as complex and time-consuming pretreatments of the samples, requirements of expensive instruments and well-trained operators, and these methods are also restricted to a limited analyte spectrum.[6] Enzyme/antibody-based immunoassay has also been developed for the detection of OPs by the readout of various electrochemical or optical transducers, such as voltammetric response,[7] surface plasmon resonance (SPR),[8] and an optical approach.[9] In recent years, SPR immunosensors have been growing rapidly. Several SPR optical biosensors have been developed for detecting low levels of pesticides residues,[10,11] for they have inherent advantages in their versatility and compatibility with label-free detection, automation, and real-time analysis. Although a high sensitivity can be achieved, the poor chemical/physical stability of the antibodies or enzymes prevents their use in harsh environments of acids or bases, organic solvents, and high temperatures. Recently, considerable effort has been devoted to replace biological receptors with synthetic counterparts as a recognition element in chemo/biosensors for the simple, rapid, selective, and sensitive detection of pesticides.[12−14] For example, new types of polymer membranes prepared using the molecular imprinting approach have been used as artificial recognition materials for conductometric sensors to sensitively detect atrazine, providing a significant easy procedure for the preparation of an herbicides sensor system with the desired selectivity and stability.[14] Sode et al. used a molecularly imprinted technology for formation of the Co^{2+}−imidazole complex on the polymers which mimicked the catalytic center of phosphotriesterase; thus, detection of OP pesticides could be achieved with high stability compared to biosensors employing enzyme as recognition element.[15] Therefore, as a recognition element, molecular imprinting polymers (MIPs) represent a new class of materials that could mimic and possibly replace their biological equivalents.

Molecular imprinting is a well-established and simple technique for the generation of recognition sites (cavities) complementary to the shape, size, and functionality of the template onto synthetic materials.[16−20] Due to the significant advantages of molecularly imprinted materials (such as mechanical/chemical stability, low cost, and easy preparation), MIPs have been used

Received: September 7, 2013
Accepted: November 22, 2013

   dx.doi.org/10.1021/ac402848x | *Anal. Chem.* XXXX, XXX, XXX−XXX

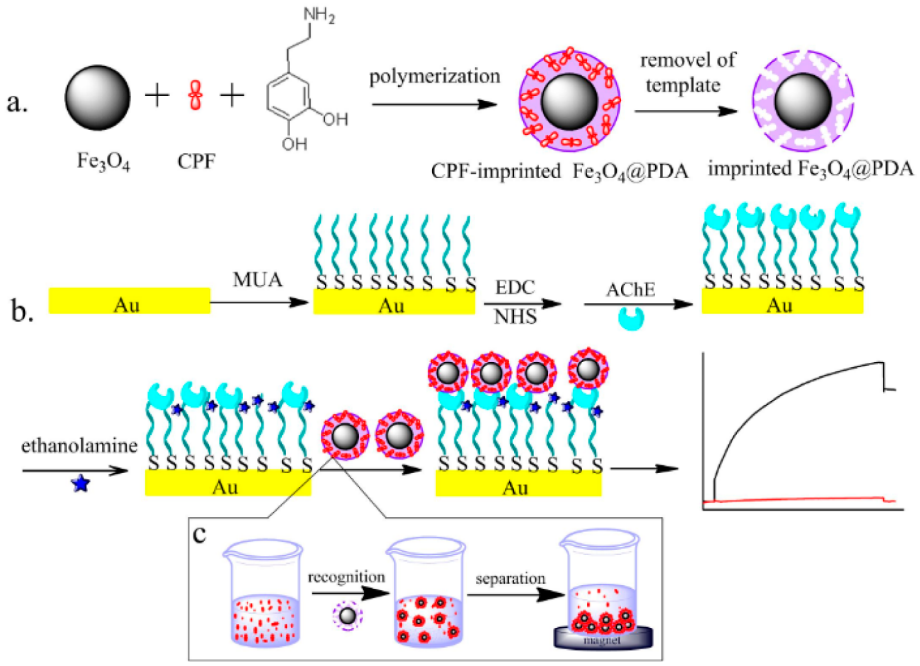

Figure 1. (a) Schematic illustration of the preparation of magnetic imprinted Fe_3O_4@PDA for CPF recognition, (b) schematic illustration of the stepwise preparation process of the sensor surface for CPF detection, and (c) illustration of recognition and separation of CPF with imprinted Fe_3O_4@PDA.

widely in many scientific and technical fields, including chromatographic separation,[21] solid-phase extraction,[22] catalysis,[23] drug-controlled release,[24] and sensors.[18,25,26] For the construction of the MIP-based sensor, in most cases, an imprinted polymer is put in physical contact with a transducer. The physicochemical response (change in mass, resistance, capacitance, refractive index, etc.) from binding a target analyte is translated into a sensor signal. This simple method, however, often leads to MIP sensors showing relatively low sensitivity and specificity.[27] One possible solution to this deficiency is to use enzyme-labeled templates to amplify the analyte-binding signal[28] and another fruitful approach is to increase the number of molecular cavities imprinted in the film.[29] Although the amount of the imprinted sites increases with the increase of the imprinted membrane thickness, thick imprinted membranes can lead to slow diffusion of the analytes to the recognition sites and to inefficient communication between the binding sites and transducers.[30] Molecular imprinting nanotechniques may provide a potential solution to these limits. Nanostructures have a small dimension with extremely high surface-to-volume ratio, and thus, more recognition sites can be imprinted, which certainly improves binding capacity of the MIPs. Many nanoparticles have been used as supports in the surface imprinting process, such as SiO_2,[31] TiO_2,[32] Fe_3O_4,[33] and quantum dots.[34] Among these widely used support nanoparticles, Fe_3O_4 particles, as special biomolecule immobilizing carriers, have gained wide attraction.[35,36] Once Fe_3O_4 particles are encapsulated inside of MIPs, the resulting polymer material will have magnetically susceptible characteristics and can be easily separated simply with the help of an external magnetic field after their performances. In recent years, magnetic MIPs have become a hotspot based on the significant advantages of magnetic separation over conventional methods[37−39] and, therefore, have promoted the development of MIPs.

Dopamine is considered as a small molecule mimic of Mefp-5 which contains the catechol and primary amine functional groups in the side chains of 3,4-dihydroxy-L-phenylalanine and lysine residues. Incubation of substrates in an alkaline dopamine solution resulted in oxidative polymerization of dopamine and formation of a heterogeneous polymer coating.[40] Inspired by this breakthrough, several studies on the preparation of MIP materials by combining the merits of surface-imprinted techniques and the self-polymerization of functional monomer dopamine have been reported.[26,41−44] However, these studies mainly focused on employing PDA-based magnetic MIPs as special molecule-immobilizing carriers for biomolecular separation. The use of MIP-capped Fe_3O_4 NPs to the SPR system as recognition element and signal amplifier has not been reported as far as we know.

In this work, we propose an approach to the synthesis of magnetic MIPs with high density and accessible recognition sites for sensitive SPR detection of chlorpyrifos (CPF). As illustrated in Figure 1, the magnetic MIPs were synthesized by self-polymerization of dopamine on the surface of Fe_3O_4 NPs in the presence of template CPF in solution. This method enables the template-imprinting sites to situate at the surface or in the proximity of material's surfaces; thus, nearly all the recognition sites are accessible to the target and fast association/dissociation kinetics (Figure 1a) can be expected. The shell thickness can be adjusted by varying the time for dopamine self-polymerization.[44] Results show that the target molecules can be rapidly enriched and separated by the imprinted Fe_3O_4@polydopamine nanoparticles (Fe_3O_4@PDA NPs) by an external magnetic field. Integrating the CPF-imprinted Fe_3O_4@PDA NPs to a SPR chip through the specific interactions between the CPF rebound in the recognition cavities in the PDA matrix and the AChE immobilized on sensor chip results in a significant signal amplification due to the high molecular weight of Fe_3O_4@PDA NPs (Figure 1b). Thus, sensitive detection of CPF can be achieved with the present approach. To our knowledge, this is the first attempt to combine magnetic molecular imprinted polymer nanoparticles with SPR for CPF detection.

dx.doi.org/10.1021/ac402848x | Anal. Chem. XXXX, XXX, XXX−XXX

EXPERIMENTAL SECTION

Synthesis of Fe_3O_4 Nanoparticles. The Fe_3O_4 NPs were prepared through the coprecipitation method as reported.[45] In brief, 2.35 g of $FeSO_4·7H_2O$ and 4.1 g of $FeCl_3·6H_2O$ were dissolved into 100 mL of ultrapure water in a flask. This mixture was stirred, followed by adding 25 mL of 25% (w/w) $NH_3·H_2O$ quickly at room temperature. The solution color altered from orange to black, leading to a black precipitate. Then, 1 mL of oleic acid was dropped into the dispersion slowly at 80 °C in 1 h. The whole process was carried out under N_2. After that, the as-synthesized Fe_3O_4 NPs were extracted from water into 30 mL of toluene. The magnetic Fe_3O_4 NPs were formed.

Preparation of Imprinted Fe_3O_4@PDA and Control Fe_3O_4@PDA NPs. Fe_3O_4 NPs (50 mg) were dissolved in 20 mL of Tris buffer (10 mM, pH = 8.0); subsequently, 5 mL of 1 mg/mL CPF acetonitrile solution was added and the mixture solution was mechanically stirred for 2 h at room temperature until well-suspended. Consequently, dopamine (25 mg) was added to the above solution in an open flask to allow for continuous oxygen supply through the water−air interface, and the reaction was continued for another 4 h at room temperature. The resultant polymers collected by the external magnet were washed with a mixture of 3% (v/v) acetic acid and 20% (v/v) acetonitrile solution, to extract the template molecules until there was no CPF that could be detected by the UV spectrometer in the rinses, and then thoroughly washed with ultrapure water. The obtained product was denoted as imprinted Fe_3O_4@PDA. For comparison, control Fe_3O_4@PDA NPs were prepared and washed using the same recipe without the template molecule in the self-polymerization stage.

Sensor Construction. A bare gold film was initially immersed in Piranha solution (containing sulphuric acid and hydrogen peroxide in a 70%/30% vol ratio) for 2 min to eliminate any possible contamination. *(CAUTION: "Piranha" solution reacts violently with organic materials; it must be handled with extreme care.)* Then, it was washed with absolute ethanol and ultrapure water, respectively, and thoroughly dried with N_2. The cleaned gold chip surface was placed on the prism with the mach oil and covered with the cuvette. Then, 50 μL of 1 mM 11-mercaptoundecanoic acid (MUA) solution was injected into the cuvette for 2 h to form a self-assembled monolayer with carboxyl functional group. After extensive rinsing with Tris buffer, 50 μL of the mixture of 0.2 M ethyl-3-(3-dimethylaminopropy-lcarbodiimide) hydrochloride (EDC) and 0.05 M *N*-hydroxysuccinimide (NHS) was injected into the cuvette for 10 min to activate the terminal carboxyl group of MUA. Subsequently, 50 μL of 2 U/mL AChE was injected after rinsing with Tris buffer and incubated for 30 min to allow the formation of covalent amide linkages. Passivation of the unused activated carboxyl groups was performed by incubating the surface with 50 μL of 1.0 M ethanolamine for 10 min. After thorough washing with Tris buffer (pH = 8.5), the fabricated AChE/MUA/gold film sensor interface was further used to detect CPF bound on the imprinted Fe_3O_4@PDA.

SPR Measurements of Molecular Recognition Properties. The sensitive detection of CPF was conducted by integrating CPF-rebound imprinted Fe_3O_4@PDA NPs to the AChE/MUA/gold film SPR sensor surface, and adjustments were made by altering the concentration of CPF added to the imprinted Fe_3O_4@PDA NPs solution. The detection procedure consisted of two steps: First, the imprinted Fe_3O_4@PDA solution was mixed with various concentrations of CPF, and the mixture was shaken on a rocking table for 12 h[42] at room temperature to form CPF-rebound imprinted Fe_3O_4@PDA NPs, which were then separated and enriched using a magnet, as illustrated in Figure 1c. Second, the CPF-rebound imprinted Fe_3O_4@PDA solution was injected into the SPR cuvette, and the solution was kept in contact with the AChE immobilized on the AChE/MUA/gold film sensor chip for association for 30 min; then, the solution was drained out with a peristaltic pump, and a 50 μL Tris buffer was injected for the dissociation measurement. These processes were performed with a self-edited semiautomatic program sequence and real-time monitored with the Data Acquisition software.

RESULTS AND DISCUSSION

Preparation and Characterization of Magnetic Imprinted Fe_3O_4@PDA NPs and Control Fe_3O_4@PDA NPs. With magnetically susceptible characteristics, high-mechanical stability, and large surface area, Fe_3O_4 NPs are ideal matrix material for the preparation of MIPs by using a surface imprinting technique.[46] During the self-polymerization of dopamine on the Fe_3O_4 NPs in the presence of CPF, the CPF molecules can be trapped in the cross-linked polymeric network due to the molecular imprinting effect. One can reasonably speculate that the residual amino or hydroxyl groups in the PDA molecule can form hydrogen bonds with the nitrogen/oxygen atom of CPF. In addition, the templates have a heteroatom ring (similar to a benzene ring) in the chemical structure. Meanwhile, there are many benzene rings in the chain of the PDA. The structure similarity gives rise to the van der Waals interaction between templates and polymers.[47] A specific spatial distribution of phenyl, OH, and NH functional groups on the imprinted Fe_3O_4@PDA NPs surface is expected, which maximizes the attractive interactions between the recognition sites and the template molecules. These favorable interactions and complementary cavities create the microenvironment for recognition of CPF molecules.

The morphology and size distribution of the obtained imprinted Fe_3O_4@PDA NPs are analyzed via TEM (Figure 2). The TEM image shows that the Fe_3O_4 NPs with a size range of 6−7 nm in diameter were of well spherical structure and high monodispersity (Figure 2A). After spontaneous deposition of a thin adherent PDA layer on the Fe_3O_4 NPs surface, the resulted Fe_3O_4@PDA NPs retained the spherical structure with an average diameter of 8−10 nm (Figure 2B). The thickness of the PDA layer was determined to be ∼1 nm. To further investigate the capture possibility of the synthesized Fe_3O_4@PDA core−shell NPs under the external magnetic field, the Fe_3O_4@PDA NPs suspension in the absence and presence of an external magnet was conducted (Figure 2C). It is clear that the Fe_3O_4@PDA NPs suspension was homogeneous and black (Figure 2C, bottle 1). Once an external magnetic field was applied, the Fe_3O_4@PDA NPs were attracted quickly toward the magnet, leaving the bulk solution clear and transparent (Figure 2C, bottle 2). These results demonstrated the excellent magnetic separation ability of the Fe_3O_4@PDA magnetic NPs, which enables the direct capture and easy separation and concentration of targets in complex samples in an external magnetic field without filtration, centrifugation, and other complex operations.

FT-IR experiments were carried out to investigate the formation of CPF-imprinted Fe_3O_4@PDA NPs. Figure 3 shows the FT-IR spectra of Fe_3O_4, PDA, control Fe_3O_4@PDA, CPF-imprinted

dx.doi.org/10.1021/ac402848x | *Anal. Chem.* XXXX, XXX, XXX−XXX

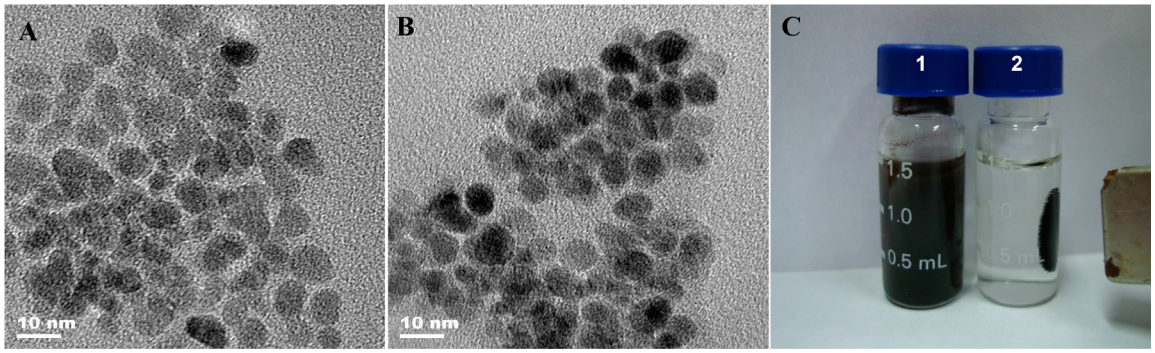

Figure 2. TEM images of (A) Fe_3O_4 NPs and (B) Fe_3O_4@PDA NPs. Photographic images of Fe_3O_4@PDA NPs in the absence (bottle 1) and presence (bottle 2) of an external magnetic field (C).

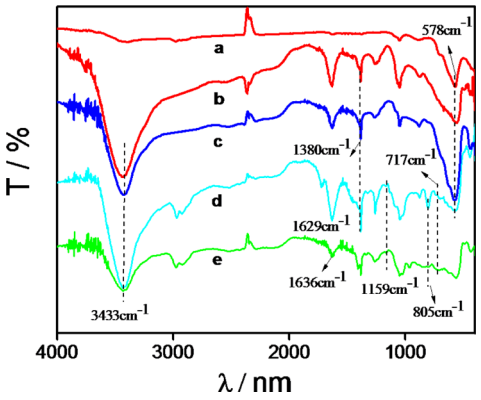

Figure 3. FT-IR spectra of (a) Fe_3O_4 NPs, (b) PDA, (C) control Fe_3O_4@PDA NPs, (d) CPF-imprinted Fe_3O_4@PDA NPs, and (e) CPF.

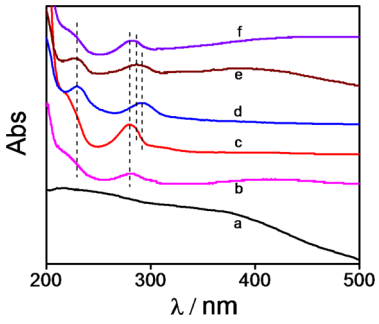

Figure 4. UV−vis absorption spectra of (a) Fe_3O_4, (b) control Fe_3O_4@PDA NPs, (c) PDA, (d) CPF, (e) CPF-imprinted Fe_3O_4@PDA NPs, and (f) imprinted Fe_3O_4@PDA NPs.

Fe_3O_4@PDA NPs, and CPF. A sharp and strong Fe−O stretching peak (~578 cm^{-1}) was observed for the bulk Fe_3O_4 (Figure 3a). In the spectrum of PDA (Figure 3b), the absorption band around 3433 cm^{-1} was ascribed to the stretching vibration of catechol −OH groups. The peaks at 1629 and 1380 cm^{-1} were attributed to the overlap of the C═C resonance vibrations in the aromatic ring and the C−N stretching modes, respectively.[48] After self-polymerization of dopamine on the Fe_3O_4 NPs surface without template, the FT-IR spectrum showed the bands for both PDA and Fe_3O_4 (Figure 3c), indicating that the PDA was indeed coated on the surface of the Fe_3O_4 NPs and the main structure of Fe_3O_4 was not changed by the modification.[46] After self-polymerization of dopamine on the surface of the Fe_3O_4 NPs in the presence of template CPF, the FT-IR spectrum of CPF-imprinted Fe_3O_4@PDA NPs (Figure 3d) exhibited the typical CPF absorption features (Figure 3e) of the stretching vibration of P−O−C bonds at 1159 cm^{-1}, stretching vibration of P═S bonds at 805 cm^{-1}, and stretching vibration of C−Cl bonds at 717 cm^{-1}, demonstrating the successful formation of CPF-imprinted Fe_3O_4@PDA NPs by the one-pot self-polymerization method.

During the self-polymerization of dopamine, CPF molecules were embedded in the PDA layer simultaneously. After removal of the embedded CPF molecules, the CPF imprinted sites will be regenerated. To confirm the removal of the templates, UV−vis spectra of Fe_3O_4, CPF, PDA, control Fe_3O_4@PDA NPs, CPF-imprinted Fe_3O_4@PDA NPs, and CPF-imprinted Fe_3O_4@PDA NPs after extraction (imprinted Fe_3O_4@PDA NPs) were compared (Figure 4). It is clear that the absorbance intensity of Fe_3O_4 NPs decreased monotonically with the increase of light wavelength in the range of 200−500 nm and no obvious absorption peak was observed (Figure 4a), which is in agreement with the results in the literature.[49] After self-polymerization of dopamine on the Fe_3O_4 NPs surface, a new absorption peak occurring at 280 nm was observed (Figure 4b) due to the absorption of PDA (Figure 4c), suggesting the successful formation of PDA layer on the surface of Fe_3O_4 NPs. Two adsorption peaks at 230 and 292 nm were obtained in the spectrum of CPF (Figure 4d), which were ascribed to the absorption of the substituents in the pyridine rings.[50] Upon incorporation of CPF into Fe_3O_4@PDA NPs, two peaks shift to 228 and 285 nm, respectively (Figure 4e), which may be due to the hydrogen bond interactions between the residual amino groups of PDA and nitrogen/oxygen atom of CPF. After extracting CPF from the CPF-imprinted Fe_3O_4@PDA NPs, a clear peak at 280 nm was observed and the peak at 228 nm nearly disappeared (Figure 4f); the UV−vis spectrum was similar to that of control Fe_3O_4@PDA NPs (Figure 4b), indicating the efficient removal of the templates upon extraction.

Electrochemical impedance spectroscopy (EIS) is an effective method to monitor the change of surface properties of electrodes.[48] The typical impedance spectrum (presented in the form of the Nyquist plot) includes a semicircle portion at higher frequencies corresponding to the electron-transfer-limited process and a linear part at lower frequency range representing the diffusion-limited process. The semicircle diameter in the impedance spectrum is equal to the electron-transfer resistance (R_{et}), which reflects the electron-transfer kinetics of the redox probe at the electrode surface. EIS had been employed to confirm the interface properties of the surfaced-modified SPR sensors, and the results are shown in Figure 5. The electrochemical

dx.doi.org/10.1021/ac402848x | Anal. Chem. XXXX, XXX, XXX−XXX

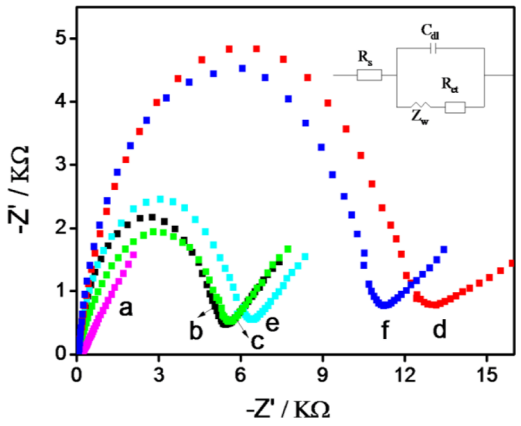

Figure 5. Nyquist plots of the different SPR sensor surfaces in a PBS solution (0.1 M, pH 7.0) containing 0.1 M KCl and 10 mM $Fe(CN)_6^{3-/4-}$: (a) bare gold film, (b) AChE/MUA/gold film, and AChE/MUA/gold film binding of (c) control Fe_3O_4@PDA NPs, (d) CPF-imprinted Fe_3O_4@PDA NPs, (e) imprinted Fe_3O_4@PDA NPs, and (f) imprinted Fe_3O_4@PDA NPs after rebinding 10 μM CPF, respectively. Inset: the equivalent circuit used to model the impedance data in the presence of the redox couple. R_s, Z_w, R_{et}, and C_{dl} represent the solution resistance, the Warburg diffusion resistance, the electron-transfer resistance, and the double layer capacitance, respectively.

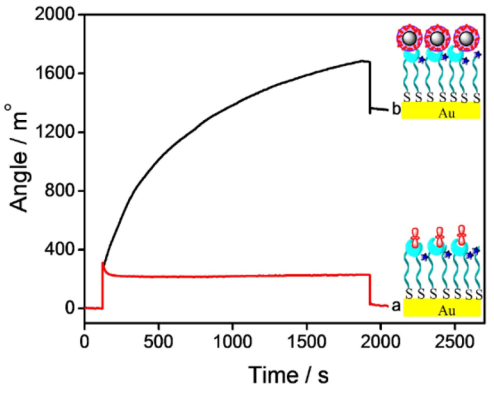

Figure 6. SPR response curve for detection of 10 μM CPF: (a) direct detection of free CPF in PBS and (b) amplification with imprinted Fe_3O_4@ PDA NPs. Inset: illustration of the sensor surface, showing the binding and amplified detection.

impedance spectrum of a bare gold film electrode showed almost a straight line, the characteristics of a mass diffusional limiting electron-transfer process (Figure 5a). After subsequent stepwise immobilization of MUA, EDC-NHS activation, and AChE and the ethanolamine blocking, the value of R_{et} increased to 5.2 KΩ (Figure 5b), which indicated the successful formation of a AChE/MUA/gold membrane, thus inhibiting the electron transfer of $[Fe(CN)_6]^{3-/4-}$ to the electrode surface by the insulating effect of proteins. Binding of control Fe_3O_4@PDA NPs to the AChE/MUA/gold film brought a negligible increase in interfacial resistance to 5.5 KΩ (Figure 5c). When the CPF-imprinted Fe_3O_4@PDA NPs were kept in contact with the AChE/MUA/gold film sensor chip for association for 30 min, as expected, the R_{et} was significantly enlarged to 12.5 KΩ (Figure 5d). These results indicated that the CPF-imprinted Fe_3O_4@PDA NPs can be bound to the surface of the AChE/MUA/gold film. When the imprinted Fe_3O_4@PDA NPs were bound to the AChE/MUA/gold film, a remarkable decrease of the interfacial resistance to 6.0 KΩ was obtained, which indicated the efficient removal of the templates upon extraction (Figure 5e). The extraction of CPF resulted in the formation of sites in the imprinted Fe_3O_4@PDA NPs that could in turn selectively rebind the template molecules. After rebinding 10 μM CPF, the resultant CPF-rebound imprinted Fe_3O_4@ PDA NPs were also bound to the AChE/MUA/gold film and the R_{et} increased dramatically, as characterized by the enlarged semicircle domains in Figure 5f, which was proximate to that of CPF-imprinted Fe_3O_4@PDA NPs (Figure 5d). These results verified that the imprinted Fe_3O_4@PDA NPs have good capability to rebind a large amount of the target molecules due to the high surface-to-volume ratio of Fe_3O_4@PDA NPs.

Magnetic Imprinted Fe_3O_4@PDA NPs Amplify the SPR Signal. To clearly show the amplification effect of the magnetic imprinted Fe_3O_4@PDA NPs, the SPR response resulting from the direct binding of CPF without imprinted Fe_3O_4@PDA NPs was also studied. After direct binding of 10 μM CPF with AChE immobilized on AChE/MUA/gold film for 30 min, only a 21.1 m° SPR angle shift was observed (Figure 6a). It should be noted that the SPR angle shift greatly increased, to 1355.7 m°, when the imprinted Fe_3O_4@ PDA NPs were used (Figure 6b), a value approximately 64 times higher than that for the direct detection format at the same CPF concentration, further demonstrating the dramatic amplification of the imprinted Fe_3O_4@PDA NPs in the SPR sensing protocol. The reasons could be attributed to two aspects: First, the imprinted Fe_3O_4@ PDA NPs gave more recognition sites for CPF on account of the high surface area of the spheroidal structure.[51] Second, the high refractive index and the high molecular weight of the Fe_3O_4 NPs might be in favor of the amplification of SPR signal.[52]

Imprinted Fe_3O_4@PDA NPs Enhanced SPR Sensing for CPF Detection. Under the optimized experimental conditions (Figure S1 in the Supporting Information), the CPF-rebound imprinted Fe_3O_4@ PDA NPs with various CPF concentrations were injected into the SPR cuvette; the analysis of different CPF concentrations is illustrated in Figure 7A. A negligible SPR angle shift was observed at 0 nM CPF (curve a), while the SPR angle shifts resulting from the binding of the imprinted Fe_3O_4@ PDA NPs gradually increased with increasing CPF concentrations (curves b–g). These results implied that the molecularly imprinted sites with PDA ligands can not interact with AChE. Only after rebound with CPF, the nucleophilic serine of AChE attacks the phosphorus atom of CPF, forming a bipyramidal transition state, which is followed by the departure of the leaving group and the formation of the phosphylserine;[53] thus, the CPF-rebound imprinted Fe_3O_4@ PDA NPs can be captured by the AChE assembled on the AChE/MUA/gold film and resulting in a enhanced SPR signal. The calibration curve between the ΔAngle and the CPF concentration was plotted in Figure 7B (curve a). As can be seen, in the high concentration range, the ΔAngle tends to be stable, indicating that the imprinting sites were almost occupied by CPF molecules. On analyzing the changes in the ΔAngle with respect to the concentration of CPF, a good linear relationship was obtained in the range of 0.001–10 μM, which is greatly improved compared with the linear ranges of 5.0×10^{-7}–1.0×10^{-5} M for the imprinted polyaminothiophenol-Au NP-glassy carbon sensor,[18] 1.0×10^{-6}–2.0×10^{-9} M for the chemiluminescence method based on the CPF-imprinted hollow particles as recognition elements,[54] and 1.5–40 nM for amperometric biosensor based on AChE/ZnS/poly(indole-5-carboxylic acid)/Au electrode.[55] With the use of the 3 S/N principle, the detection limit was determined to be 0.76 nM, which is much lower than those

dx.doi.org/10.1021/ac402848x | Anal. Chem. XXXX, XXX, XXX–XXX

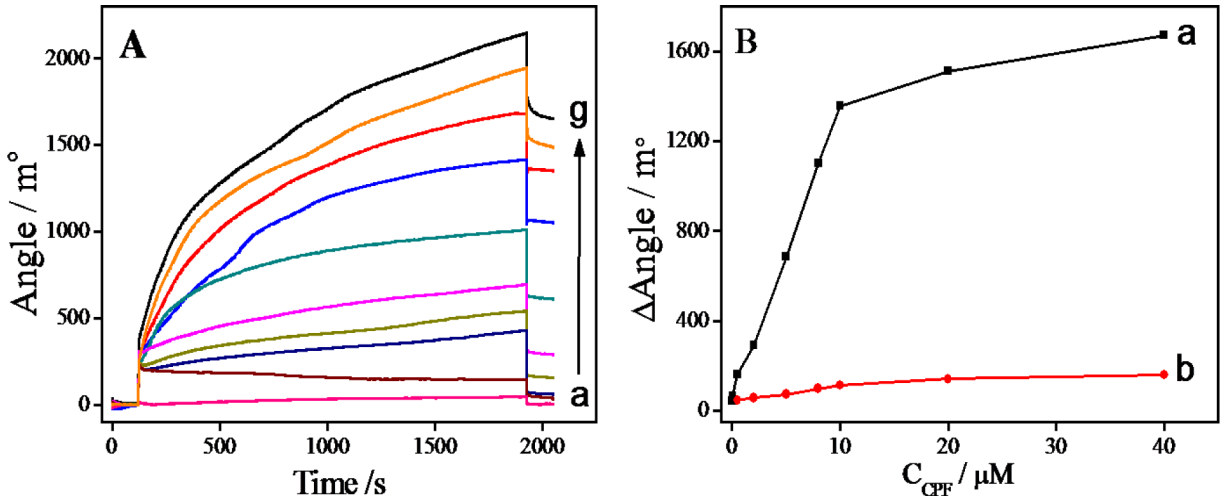

Figure 7. (A) SPR sensorgrams of imprinted Fe_3O_4@PDA NPs binding to the AChE/MUA/gold chip after rebinding different concentrations of CPF, curves a−g represent 0, 0.001, 0.05, 0.5, 2, 5, 8, 10, 20, and 40 μM CPF. (B) Calibration plots of the ΔAngle verse CPF concentration for the SPR sensor based on (a) imprinted Fe_3O_4@PDA NPs and (b) control Fe_3O_4@PDA NPs.

reported at 0.33 μM,[18] 0.92 nM,[54] and 1.5 nM.[55] The amplification effect of the magnetic imprinted Fe_3O_4@PDA NPs was further confirmed by the control experiments of Fe_3O_4@PDA NPs under the same experimental conditions (curve b). It is clear that the ΔAngle resulting from the interaction between the control Fe_3O_4@PDA NPs and variable concentrations of CPF were substantially lower, suggesting the lower binding affinity of CPF to control Fe_3O_4@PDA NPs. The slight increase in the SPR angle is due to nonspecific binding of the CPF onto the control Fe_3O_4@PDA NPs. The higher SPR angle shift and the lower detection limit by the imprinted Fe_3O_4@PDA NPs should be attributed to the formation of the molecularly imprinted sites on the surface of Fe_3O_4 NPs that provide molecular structural contours and PDA ligands for the steric accommodation of the CPF substrate. Thus, the steric fit of CPF to the imprinted sites increased the binding affinity of CPF to the imprinted Fe_3O_4@PDA NPs, resulting in a huge change of SPR signal.

Selectivity of the Magnetic Imprinted Fe_3O_4@PDA NP-Based SPR Sensor. Selectivity is the ability of the sensor to discriminate between different analytes. Thus, in order to test the binding selectivity of magnetic imprinted Fe_3O_4@PDA NPs, a sensing experiment was conducted using different but structurally analogous compounds, such as dimethoate, fenitrothion, and propazine (Figure S2 in the Supporting Information shows the structural formulas of the pesticide compounds). As shown in Figure 8, CPF resulted in the largest response among the tested pesticides on the magnetic imprinted Fe_3O_4@PDA NP-based SPR sensor. For the SPR sensor, selectivity efficiency is defined by the following equation: selectivity efficiency = $\Delta R_{analogues}/\Delta R_{CPF}$. Here, ΔR is the difference of SPR angle shifts upon addition of imprinted Fe_3O_4@PDA after rebinding pesticides. According to the equation, the selectivity efficiencies of CPF, dimethoate, fenitrothion, and propazine were calculated to be 1.0, 0.1, 0.04, and 0.06, respectively. These results implied that CPF-imprinted Fe_3O_4@PDA NPs after extraction exhibited high selectivity for CPF, but the SPR angle shifts on the control Fe_3O_4@PDA NP-based SPR sensor for CPF, dimethoate, fenitrothion, and propazine were very low and nearly identical. The outstanding selectivity of the sensor could be attributed to the robust imprinted sites or cavities of the imprinted Fe_3O_4@PDA NPs that retained precisely the memory of the size, shape, and orientation of chemical functionality of the template molecule CPF.

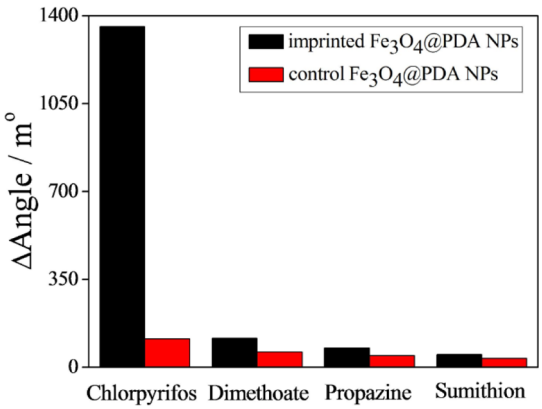

Figure 8. Binding behaviors of 10 μM chlorpyrifos, dimethoate, propazine, and sumithion on the imprinted Fe_3O_4@PDA NPs and control Fe_3O_4@PDA NPs.

Detection of CPF Residues in Agricultural Products. The excellent specificity and high sensitivity of the sensor suggest that the developed method might be directly applied for detecting pesticide residues in real samples. Therefore, we further investigated whether the sensing strategy described here could be utilized to monitor the residues of CPF in agricultural products such as apples. The apple sample was prepared as reported with slight modifications.[2] Briefly, the apple samples were first chopped, and the edible parts of the apple samples were crushed into a homogenate. A total of 20 g of homogenate was mixed with 20 mL of acetonitrile, and the resulting mixture was shaken for 20 min and then filtered to remove the insoluble draff. Subsequently, the extract solution of apple samples was spiked with CPF standard solution at a number of concentrations spanning the range of 0.1−10 μM, and then, the spiked apple samples were mixed with imprinted Fe_3O_4@PDA NPs to form CPF-rebound Fe_3O_4@PDA NPs for SPR measurements. As shown in Table 1, satisfactory recoveries ranging from 93% to 104% were obtained, which is an indicator of its good accuracy and practicability for use with real samples.

dx.doi.org/10.1021/ac402848x | Anal. Chem. XXXX, XXX, XXX−XXX

Table 1. Analytical Results of CPF in Apples (n = 3)

	content of CPF (μM)	add (μM)	found (μM)	recovery (%)
1	none	0.1	0.093	93
2	none	2	2.09	104
3	none	10	10.1	101

CONCLUSIONS

In this work, we have demonstrated a sensitive SPR sensing protocol based on a magnetic surface imprinting technique for the detection of organophosphate pesticide for the first time. The core−shell magnetic imprinted Fe_3O_4@PDA NPs are prepared by a facile approach based on self-polymerization of dopamine in the presence of template CPF on the Fe_3O_4 NPs surface. The obtained imprinted Fe_3O_4@PDA NP sphere nanostructures show the excellent magnetic properties of Fe_3O_4 core, allowing for the direct capture and easy concentration and separation of targets in complex samples in an external magnetic field, and the high surface-to-volume ratios of Fe_3O_4 NPs allow for increasing the number and ratio of imprinted sites that are accessible for binding and, therefore, binding capacity of the imprinted Fe_3O_4@PDA NPs. In addition, the controllable membrane-forming ability of PDA shell facilitates the situation of the imprinted sites on the surface of Fe_3O_4 NPs, which can provide fast association/dissociation kinetics for template recognition. Therefore, sensitive and selective detection of CPF was achieved by employing the imprinted Fe_3O_4@PDA as both an amplifier to increase the SPR signal and a special recognition element to improve the selectivity due to its high refractive indices, high molecular weights, and imprinted effect. The wide response range, excellent sensitivity and selectivity, and high stability of the designed biosensor make this magnetic imprinted Fe_3O_4@PDA an attractive recognition element for various SPR sensors for detecting pesticide residuals and other environmentally deleterious chemicals.

ASSOCIATED CONTENT

Supporting Information

Experimental details in the form of text are given for the reagents, apparatus, and optimization of experimental conditions; the figures are provided for optimization of experimental conditions and structural formulas of the pesticide compounds. This material is available free of charge via the Internet at http://pubs.acs.org.

AUTHOR INFORMATION

Corresponding Author

*Phone: +86-791-8396-9518. Fax: +86-791-8396-9518. E-mail: jdqiu@ncu.edu.cn.

Notes

The authors declare no competing financial interest.

ACKNOWLEDGMENTS

This work was supported by grants from the National Natural Science Foundation of China (21065006, 21163014, and 21265012) and the Program for New Century Excellent Talents in University (NCET-11-1002).

REFERENCES

(1) Liu, G. D.; Lin, Y. H. *Anal. Chem.* **2005**, *77*, 5894−5901.
(2) Zhang, K.; Mei, Q. S.; Guan, G. J.; Liu, B. H.; Wang, S. H.; Zhang, Z. P. *Anal. Chem.* **2010**, *82*, 9579−9586.
(3) Sinha, S. N.; Pal, R.; Dewan, A.; Mansuri, M. M.; Saiyed, H. N. *Int. J. Mass Spectrom.* **2006**, *253*, 48−57.
(4) Cappiello, A.; Famiglini, G.; Palma, P.; Mangani, F. *Anal. Chem.* **2002**, *74*, 3547−3554.
(5) Salm, P.; Taylor, P. J.; Roberts, D.; de Silva, J. *J. Chromatogr., B* **2009**, *877*, 568−574.
(6) Zhao, W.; Ge, P. Y.; Xu, J. J.; Chen, H. Y. *Environ. Sci. Technol.* **2009**, *43*, 6724−6729.
(7) Kandimalla, V. B.; Ju, H. X. *Chem.—Eur. J.* **2006**, *12*, 1074−1080.
(8) Huang, X.; Tu, H. Y.; Zhu, D. H.; Du, D.; Zhang, A. D. *Talanta* **2009**, *78*, 1036−1042.
(9) Prabhakar, N.; Sumana, G.; Arora, K.; Singh, H.; Malhotra, B. D. *Electrochim. Acta* **2008**, *53*, 4344−4350.
(10) Mauriz, E.; Calle, A.; Lechuga, L. M.; Quintana, J.; Montoya, A.; Manclus, J. J. *Anal. Chim. Acta* **2006**, *561*, 40−47.
(11) Lin, T. J.; Huang, K. T.; Liu, C. Y. *Biosens. Bioelectron.* **2006**, *22*, 513−518.
(12) Liang, R. N.; Song, D. A.; Zhang, R. M.; Qin, W. *Angew. Chem., Int. Ed.* **2010**, *49*, 2556−2559.
(13) Marx, S.; Zaltsman, A.; Turyan, I.; Mandler, D. *Anal. Chem.* **2004**, *76*, 120−126.
(14) Piletsky, S. A.; Piletskaya, E. V.; Elgersma, A. V.; Yano, K.; Karube, I. *Biosens. Bioelectron.* **1995**, *10*, 959−964.
(15) Yamazaki, T.; Yilmaz, E.; Mosbach, K.; Sode, K. *Anal. Chim. Acta* **2001**, *435*, 209−214.
(16) Tan, C. J.; Chua, H. G.; Ker, K. H.; Tong, Y. W. *Anal. Chem.* **2008**, *80*, 683−692.
(17) Zimmerman, S. C.; Zharov, I.; Wendland, M. S.; Rakow, N. A.; Suslick, K. S. *J. Am. Chem. Soc.* **2003**, *125*, 13504−13518.
(18) Xie, C. G.; Li, H. F.; Li, S. Q.; Wu, J.; Zhang, Z. P. *Anal. Chem.* **2010**, *82*, 241−249.
(19) Liu, J. X.; Chen, H.; Lin, Z.; Lin, J. M. *Anal. Chem.* **2010**, *82*, 7380−7386.
(20) Gao, D. M.; Zhang, Z. P.; Wu, M. H.; Xie, C. G.; Guan, G. J.; Wang, D. P. *J. Am. Chem. Soc.* **2007**, *129*, 7859−7866.
(21) Tamayo, F. G.; Martin-Esteban, A. *J. Chromatogr., A* **2005**, *1098*, 116−122.
(22) Fang, G. Z.; Tan, J.; Yan, X. P. *Anal. Chem.* **2005**, *77*, 1734−1739.
(23) Liu, J. Q.; Wulff, G. *J. Am. Chem. Soc.* **2008**, *130*, 8044−8054.
(24) Gong, C. B.; Wong, K. L.; H. W. Lam, M. *Chem. Mater.* **2008**, *20*, 53−1358.
(25) Ton, X. A.; Tse Sum Bui, B.; Resmini, M.; Bonomi, P.; Dika, I.; Soppera, O.; Haupt, K. *Angew. Chem., Int. Ed.* **2013**, *52*, 1−6.
(26) Zhou, W. H.; Tang, S. F.; Yao, Q. H.; Chen, F. R.; Yang, H. H.; Wang, X. R. *Biosens. Bioelectron.* **2010**, *26*, 585−589.
(27) Ye, L.; Mosbach, K. *J. Am. Chem. Soc.* **2001**, *123*, 2901−2902.
(28) Li, J. P.; Jiang, F. Y.; Wei, X. P. *Anal. Chem.* **2010**, *82*, 6074−6078.
(29) Sharma, P. S.; Dabrowski, M.; D'Souza, F.; Kutner, W. *TrAC, Trends Anal. Chem.* **2013**, *51*, 146−157.
(30) Riskin, M.; Tel-Vered, R.; Bourenko, T.; Granot, E.; Willner, I. *J. Am. Chem. Soc.* **2008**, *130*, 9726−9733.
(31) Descalzo, A. B.; Somoza, C.; Moreno-Bondi, M. C.; Orellana, G. *Anal. Chem.* **2013**, *85*, 5316−5320.
(32) Shen, X. T.; Zhu, L. H.; Li, J.; Tang, H. Q. *Chem. Commun.* **2007**, *11*, 1163−1165.
(33) Zhang, Y.; Liu, R. J.; Hu, Y. L.; Li, G. K. *Anal. Chem.* **2009**, *81*, 967−976.
(34) Wang, H. F.; He, Y.; Ji, T. R.; Yan, X. P. *Anal. Chem.* **2009**, *81*, 1615−1621.
(35) Lawruk, T. S.; Gueco, A. M.; Mihaliak, C. A.; Dolder, S. C.; Dial, G. E.; Herzog, D. P.; Rubio, F. M. *J. Agric. Food Chem.* **1996**, *44*, 2913−2918.
(36) Tudorache, M.; Co, M.; Lifgren, H.; Emneus, J. *Anal. Chem.* **2005**, *77*, 7156−7162.
(37) Tan, C. J.; Tong, Y. W. *Anal. Chem.* **2007**, *79*, 299−306.
(38) Wang, X.; Wang, L. Y.; He, X. W.; Zhang, Y. K.; Chen, L. X. *Talanta* **2009**, *78*, 327−332.

(39) Chen, L. G.; Liu, J.; Zeng, Q. L.; Wang, H.; Yu, A. M.; Zhang, H. Q.; Ding, L. *J. Chromatogr., A* **2009**, *1216*, 3710−3719.
(40) Lee, H.; Dellatore, S. M.; Miller, W. M.; Messersmith, P. B. *Science* **2007**, *318*, 426−430.
(41) Chen, T.; Shao, M. W.; Xu, H. Y.; Zhuo, S. J.; Liu, S. S.; Lee, S. T. *J. Mater. Chem.* **2012**, *22*, 3990−3996.
(42) Zhang, M.; Zhang, X. H.; He, X. W.; Chen, L. X.; Zhang, Y. K. *Nanoscale* **2012**, *4*, 3141−3147.
(43) Ouyang, R. Z.; Lei, J. P.; Ju, H. X. *Nanotechnology* **2010**, *21*, 185502.
(44) Zhou, W. H.; Lu, C. H.; Guo, X. C.; Chen, F. R.; Yang, H. H.; Wang, X. R. *J. Mater. Chem.* **2010**, *20*, 880−883.
(45) Wu, Y. P.; Zhang, T.; Zheng, Z. H.; Ding, X. B.; Peng, Y. X. *Mater. Res. Bull.* **2010**, *45*, 513−517.
(46) Kan, X. W.; Zhao, Q.; Shao, D. L.; Geng, Z. R.; Wang, Z. L.; Zhu, J. J. *J. Phys. Chem. B* **2010**, *114*, 3999−4004.
(47) Zhao, Y. Y; Ma, Y. X.; Li, H.; Wang, L. Y. *Anal. Chem.* **2012**, *84*, 386−395.
(48) Wang, G. F.; Huang, H.; Zhang, G.; Zhang, X. J.; Fang, B.; Wang, L. *Langmuir* **2011**, *27*, 1224−1231.
(49) Tang, D. P.; Yuan, R.; Chai, Y. Q. *J. Phys. Chem. B* **2006**, *110*, 11640−11646.
(50) Bootharaju, M. S.; Pradeep, T. *Langmuir* **2012**, *28*, 2671−2679.
(51) Pan, J. M.; Yao, H.; Xu, L. C.; Ou, H. X.; Huo, P. W.; Li, X. X.; Yan, Y. S. *J. Phys. Chem. C* **2011**, *115*, 5440−5449.
(52) Wang, J. L.; Munir, A.; Zhu, Z. Z.; Zhou, H. S. S. *Anal. Chem.* **2010**, *82*, 6782−6789.
(53) Mercey, G.; Verdelet, T.; Renou, J.; Kliachyna, M.; Baati, R.; Nachon, F.; Jean, L.; Renard, P. Y. *Acc. Chem. Res.* **2012**, *45* (5), 756−766.
(54) Xie, C. G.; Li, H. F.; Li, S. Q.; Gao, S. *Microchim. Acta* **2011**, *174*, 311−320.
(55) Chauhan, N.; Narang, J.; Pundir, C. S. *Biosens. Bioelectron.* **2011**, *29*, 82−88.